

Probing Local Force Propagation in Tensed Fibrous Gels

Shahar Goren, Maayan Levin, Guy Brand, Ayelet Lesman,* and Raya Sorkin*

Fibrous hydrogels are a key component of soft animal tissues. They support cellular functions and facilitate efficient mechanical communication between cells. Due to their nonlinear mechanical properties, fibrous materials display non-trivial force propagation at the microscale, that is enhanced compared to that of linear-elastic materials. In the body, tissues are constantly subjected to external loads that tense or compress them, modifying their micro-mechanical properties into an anisotropic state. However, it is unknown how force propagation is modified by this isotropic-to-anisotropic transition. Here, force propagation in tensed fibrin hydrogels is directly measured. Local perturbations are induced by oscillating microspheres using optical tweezers. 1-point and 2-point microrheology are combined to simultaneously measure the shear modulus and force propagation. A mathematical framework to quantify anisotropic force propagation trends is suggested. Results show that force propagation becomes anisotropic in tensed gels, with, surprisingly, stronger response to perturbations perpendicular to the axis of tension. Importantly, external tension can also increase the range of force transmission. Possible implications and future directions for research are discussed. These results suggest a mechanism for favored directions of mechanical communication between cells in a tissue under external loads.

1. Introduction

Soft animal tissues are structured by the extracellular matrix (ECM),^[1] a branched network of fibers, to which cells adhere. The fibrous materials that compose the ECM have remarkable nonlinear properties^[2,3]—for example, unlike most synthetic materials, the ECM can undergo very large deformations and recover without damage due to strain stiffening.^[4] Cells can modify the ECM by applying local forces,^[5,6] and also respond to the ECM mechanical properties.^[7–9] Due to its role in many biological processes,^[8,10–12] the mechanical properties of the ECM has been extensively studied.

Over the last decades, it was found that during processes such as blood vessel growth,^[13] wound healing,^[14] and cancer metastasis,^[15,16] cells communicate their position and orientation, and sense other nearby cells or rigid boundaries. They do so by applying contractile forces and sensing the mechanical environment.

Hence, mechanical signals emerged as a

well-recognized type of cellular communication. The nonlinear mechanics of the ECM was shown to facilitate and enhance mechanical communication between cells.^[17–19] Nonlinear materials can exhibit non-trivial, longer-ranged force propagation properties that facilitate efficient cell–cell interactions.^[20–24] In an organism, fibrous materials are constantly subjected to external and internal stresses due to body posture and movement, blood flow and muscle contraction.^[25] External tension affects various cellular processes. For example, it affects cell migration in wound closure,^[26,27] and can facilitate muscle^[28] and blood vessel^[29] development. These effects are often attributed to the nonlinear mechanical response of the underlying scaffold to external tension. Tension can cause fibrous materials to align and stiffen, and thus direct cell behavior. However, it is unknown how these tension-induced alignment and stiffening effects are manifested in the microscale mechanics that cells feel, and in particular, their effect on the propagation of mechanical signals is unknown. We have recently shown that the anisotropic state of the material under tension is a critical parameter that determines the capacity of fibrous networks to transmit displacements away from their source,^[23] motivating a closer look at the anisotropy induced by tension and its relationship to force propagation, and ultimately to cell–cell communication.


Bulk shear rheology using a rheometer is the most prominent method to characterize the nonlinear mechanical properties

S. Goren, M. Levin, G. Brand, R. Sorkin
School of Chemistry
Raymond & Beverly Sackler Faculty of Exact Sciences
Tel Aviv University
P.O. Box 39040, Tel Aviv 6997801, Israel
E-mail: rsorkin@tauex.tau.ac.il

S. Goren, A. Lesman
School of Mechanical Engineering
The Iby and Aladar Fleischman Faculty of Engineering
Tel Aviv University
P.O. Box 39040, Tel Aviv 6997801, Israel
E-mail: ayeletlesman@tauex.tau.ac.il

S. Goren, M. Levin, A. Lesman, R. Sorkin
Center for Physics and Chemistry of Living Systems
Tel Aviv University
P.O. Box 39040, Tel Aviv 6997801, Israel

S. Goren, R. Sorkin
Center for Light-Matter Interactions
Tel Aviv University
P.O. Box 39040, Tel Aviv 6997801, Israel

 The ORCID identification number(s) for the author(s) of this article can be found under <https://doi.org/10.1002/smll.202202573>.

© 2022 The Authors. Small published by Wiley-VCH GmbH. This is an open access article under the terms of the Creative Commons Attribution-NonCommercial-NoDerivs License, which permits use and distribution in any medium, provided the original work is properly cited, the use is non-commercial and no modifications or adaptations are made.

DOI: 10.1002/smll.202202573

of fibrous materials.^[2,30–34] Bulk rheology studies have found that all biological fibrous materials stiffen under shear and tension,^[2] and that under compression, there are both softening and stiffening regimes.^[30] The leading suggested mechanisms that may account for this rich behavior are the alignment of fibers under tension,^[18,35–37] buckling of fibers under compression,^[38–40] and bending-to-stretching rigidity transition arising from the low-connectivity topology of these networks.^[41,42] However, despite the ability of rheometers to probe the non-linearity of fibrous materials, they can only do so at the macroscopic scale of the gel as a whole, and do not provide direct information on the mechanics at the microscale. Thus, despite accumulated knowledge on the macro-mechanical and biological consequences of external tension, there is not yet a good understanding of how tension affects the mechanical micro-environment in which cells function. In addition, bulk rheology does not provide any direct information on the propagation of mechanical signals.

A more recent approach to the study of mechanical properties of fibrous materials is microrheology. Microrheology allows inferring the viscoelastic properties of a material from the movement of micro-particles embedded in it.^[43] Microrheological techniques are categorized as either passive or active, depending on whether thermal fluctuations or active external forces drive the particles.^[44] Yet another distinction is between 1-particle methods, which track only single-particle displacements, and 2-particle methods, in which correlations between pairs of particles are used to determine the medium viscoelastic properties. Microrheology readily provides microscopic mechanical viscoelastic information. Also, microrheology is a natural tool to study the propagation of mechanical signals due to its access to local forces and displacements. However, it is usually used to study the linear response regime, and does not provide access to the nonlinear response, which are only triggered at large deformations.

Previous microrheology studies have focused on characterizing the mechanics of biological gels such as collagen, fibrin, and actin under different preparation conditions^[45–47] or during different stages of their formation.^[48–50] Others have also used 1-particle microrheology to show how local stiffness of fibrous gels is modified by cell contractility^[51,52] or internal shear.^[53,54] Few works have also fabricated and characterized anisotropic fibrous gels.^[55,56] However, none of these studies quantitatively characterized force transmission in the deformed environment.

Here we develop a novel experimental technique to probe the microscale nonlinear mechanical properties of fibrin gels. Fibrin, being the main structural component of blood clots,^[33,57,58] is a relevant model for wound healing environments, in which cells need to communicate in order to orchestrate the healing reaction. We combine a method to apply controlled stretch to soft fibrous gels with optical tweezers active microrheology. Our approach is to use external tension to trigger a nonlinear mechanical response in the material, leading to a mechanically anisotropic microenvironment. We then use microrheology together with fluorescence confocal microscopy to characterize the modified microenvironment and force transmission. We quantitatively analyze force transmission in fibrin gels under tension, providing a

framework for characterizing anisotropic materials' response to local perturbations. Our goal is to explore the relationship between tension, fiber alignment, and force transmission, improve the understanding of the role of external tension in biological processes, and promote the development of better models of fibrous materials. Overall, we show that tension leads to anisotropy in the local stiffness and in force transmission. We observe enhanced material response in tensed materials, and discuss possible causes and implications.

2. Results

2.1. Fibrin Gels are Predominantly Elastic

The fibrin gels in this study have a fibrin concentration of 0.25 mg mL⁻¹. Using confocal microscopy and image analysis, we found the gels to have a mean pore size around 6 μm, with some pores as large as 15 μm (Figure S2, Supporting Information).

We first perform bulk rheology measurements to assert that fibrin gels are solid under the chosen preparation conditions, and characterize their macroscopic linear and nonlinear shear modulus. As can be seen in **Figure 1A**, we find characteristic stiffness of ≈0.7 Pa, with solid-like viscoelastic behavior ($G' > G''$). At strains of ≈20%, nonlinear strain-stiffening begins. Our measured G values and stiffening trends are in line with previous findings.^[2,33] Here, stiffness increases by about a factor of 4 at shear strains of around 100%. We hypothesized that this strain-stiffening behavior is related to fiber alignment and is manifested at the microscale by anisotropic mechanics. **Figure 1B** depicts the frequency dependence of the shear modulus, for bulk rheology (for 5% strain) and 1- and 2-particle passive microrheology of isotropic gels. For all three methods, we observe a crossover between G' and G'' as was found in other studies.^[59] Below the crossover, we observe a plateau in G' , corresponding to a stable gel regime. All three methods give similar values of G' for low frequencies. The crossover between G' and G'' curves also occurs at a slightly different frequency for each method, meaning that their relative sensitivity to the elastic and viscous components is somewhat different. The fact that 1-particle and 2-particle methods yield similar values of G' at low frequencies is not trivial,^[60] and implies that the beads are strongly coupled to the fibers, so single bead thermal fluctuations are sensitive to the gel mechanics rather than to local interactions between the fibers and solvent. Another interesting observation is that compared to bulk rheology, G'' is negligible compared to G' in passive microrheology for low frequencies. It seems that microrheology is insensitive to viscous friction between the fibers and the solvent because of the large pore sizes of the gel. For low frequencies (below 10 Hz), the gel can be considered as an elastic solid that is merely stabilized by the solvent, but whose mechanics is dominated by the elastic network, as far as bead dynamics are concerned. We thus focus on low frequencies (frequency $f = 0.5$ –Hz, angular frequency $\omega \approx 3$ –Hz) and assume $G = G'$ with negligible frequency dependence.

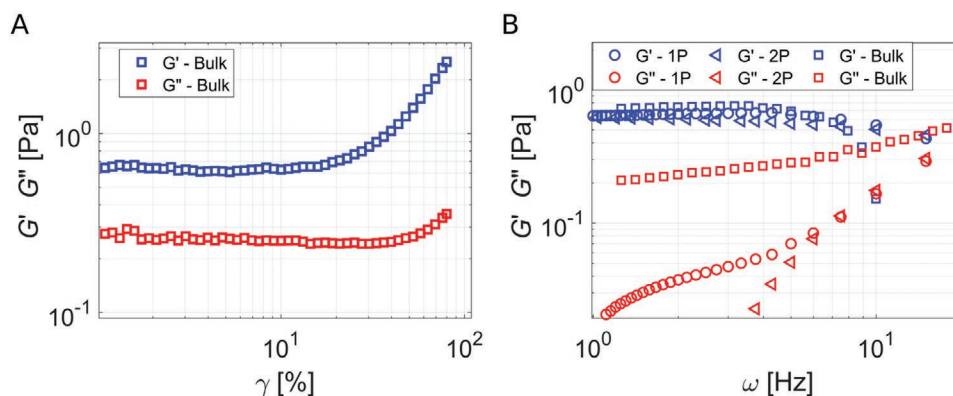


Figure 1. Bulk rheology and passive microrheology. A) The viscoelastic modulus of fibrin under increasing shear strain, showing characteristic stiffening. Strain frequency is 0.5 Hz. B) Frequency dependence of the viscoelastic modulus from bulk rheology, 1-particle and 2-particle passive microrheology. The data shown is representative. Data with errors is shown in Figure S13, Supporting Information.

2.2. Tension-Induced Transition from Isotropic to Anisotropic State

Fluorescence microscopy shows substantial fiber alignment in the x -direction in tensed gels, and isotropic distribution of fiber orientations in untensed gels, as seen in Figure 2A,B. Stretching the fibrous network also leads to contraction in the y - and z -directions, and therefore the overall density of fibers in the field of view is higher for tensed gels (see Figure S5, Supporting Information). Figure 2C,D shows the distribution of orientations from which the nematic order parameter is

computed. Tension leads to a large fraction of fibers aligned in the x -direction, and a peak is observed in $\theta = 0$ for tensed gels. Confocal images are scanned line by line, which introduces spurious directionality in the line-scanning direction. Most images in this study were recorded with x as the scanning axis, and as can be seen in the Figure 2C, a small peak appears for untensed gels as well. We correct for this effect by quantifying and subtracting it as described in Figure S6, Supporting Information. Figure 2E compares the distribution of the NOP for untensed and tensed gels, demonstrating the transition from isotropic to anisotropic state due to tension.

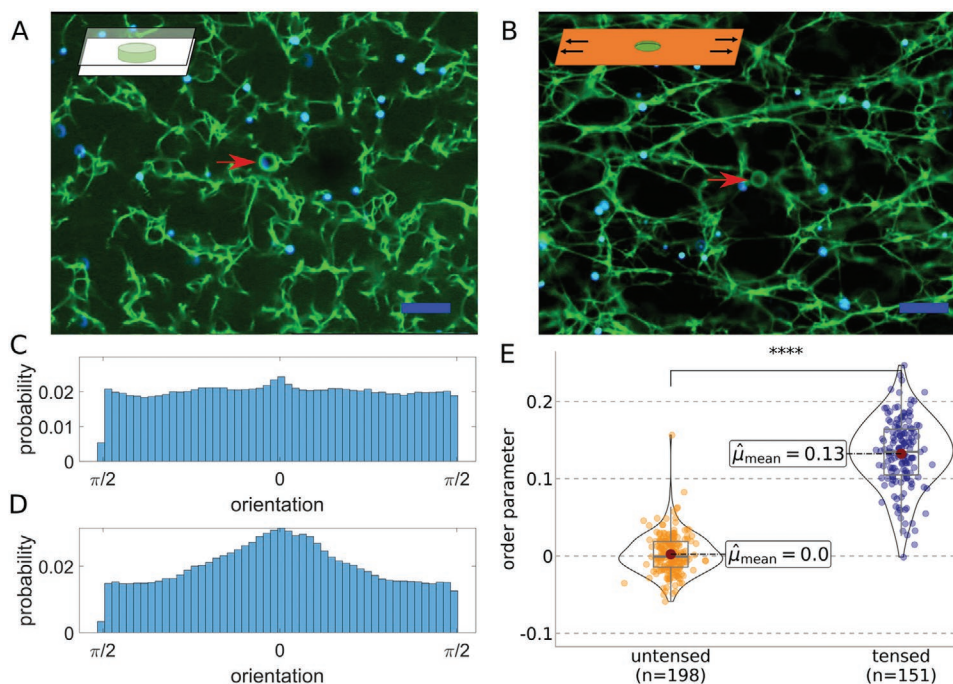


Figure 2. Confocal fluorescence microscopy shows fiber alignment in tensed gels. A) Untensed and B) tensed gels confocal scans. Driven bead is pointed with an arrow in the center, and tracer beads are shown in blue. Insets describe the sample loading conditions for each type. Scale bar: 10 μm . C,D) The orientation distribution for untensed and tensed gels is displayed, respectively. E) Comparison of the distributions of order parameter NOP = $\langle \cos(2\theta) \rangle$ computed over the directions of intensity gradients in image scans in untensed and tensed gels.

2.3. Tension-Induced Stiffness Anisotropy Measured by 1-Point Active Microrheology

We perform 1-point active microrheology measurements to quantify the modification in stiffness and mechanical anisotropy as a result of external tension. To obtain the shear modulus, we assume the gel is incompressible (with Poisson ratio $\nu = 1/2$), as was shown in previous studies.^[46,61] We compare compressible and incompressible expressions in Equations (S1), (S4), (S5), and (S6), Supporting Information. Video S1, Supporting Information, shows how the network deforms during a microrheology experiment, as explained in Experimental Section. It displays a driven bead (dark spot in the center) oscillating and deforming the fibrous network (green) and the tracer beads (orange) around it. It clearly shows how the oscillations propagate the network. Microrheology experiments are done as described in Experimental Section. Videos S2 and S3, Supporting Information, are examples of recordings that were used for quantification of 1-point and 2-point microrheology.

From the driven bead amplitude we obtain the local shear modulus using Equation (1). **Figure 3A,B** compares the distributions of shear moduli in x - and y -directions for untensed gels and tensed gels, respectively. It can be seen that for untensed gels, an average stiffness value of $\approx 0.44 \pm 0.36$ Pa is found. Untensed gels are isotropic, with their distributions for x and y shear moduli indistinguishable (Kolmogorov–Smirnov, $P_{KS} = 0.44$). For tensed gels we observe distinctly different distributions for x and y ($P_{KS} < 10^{-4}$) directions with moduli of $\approx 16 \pm 14$ Pa in the direction of tension (x) and $\approx 9 \pm 8$ Pa in the perpendicular direction (y). This corresponds to a remarkable stiffening of 20–40 fold compared to untensed gels. The mechanical anisotropy, that is, the ratio G_y/G_x decreases from 1 in untensed

gels to $\approx 0.62 \pm 0.27$ on average in tensed gels (Figure 3C). Our results demonstrate that tension leads to a dramatic increase in stiffness in all directions, and a moderate anisotropic effect. Figure 3D depicts the mechanical anisotropy ratio G_y/G_x and its dependency on the local fiber alignment in the vicinity of the driven bead. It can be seen that fiber alignment is a predictor of mechanical anisotropy, for both untensed and tensed gels.

We emphasize that embedded microsphere dynamics is coupled to those of the fibrin network due to the following reasons: first, despite its low concentration, fibrin still forms a branched network that is stable under the forces applied in the experiment. Second, both driven and tracer beads in the experiment adhere strongly to the fibers. It can be seen in confocal images that beads are only present on fibers and not in pores (Figure 2A,B, Video S1, Supporting Information). Also, during the experiments it was very rare to see freely moving beads, despite the pulling force of the optical trap, and these rare events were precluded from analysis. It was also reported previously that polystyrene beads tend to adhere firmly to fibrin.^[62] Therefore, the beads are strongly coupled to the network. Last, our experiments focus on the low frequency regime (≈ 1 Hz), in which the medium is predominantly elastic, as seen by bulk rheology (Figure 1). Thus, the measured bead dynamics reflect the elastic shear modulus of the gel.

2.4. Force Transmission of Untensed and Tensed Gels Measured with 2-Point Active Microrheology

2-point active microrheology experiments are performed by oscillating one bead and measuring the response amplitude of other beads in its vicinity. A crucial assumption in our analysis

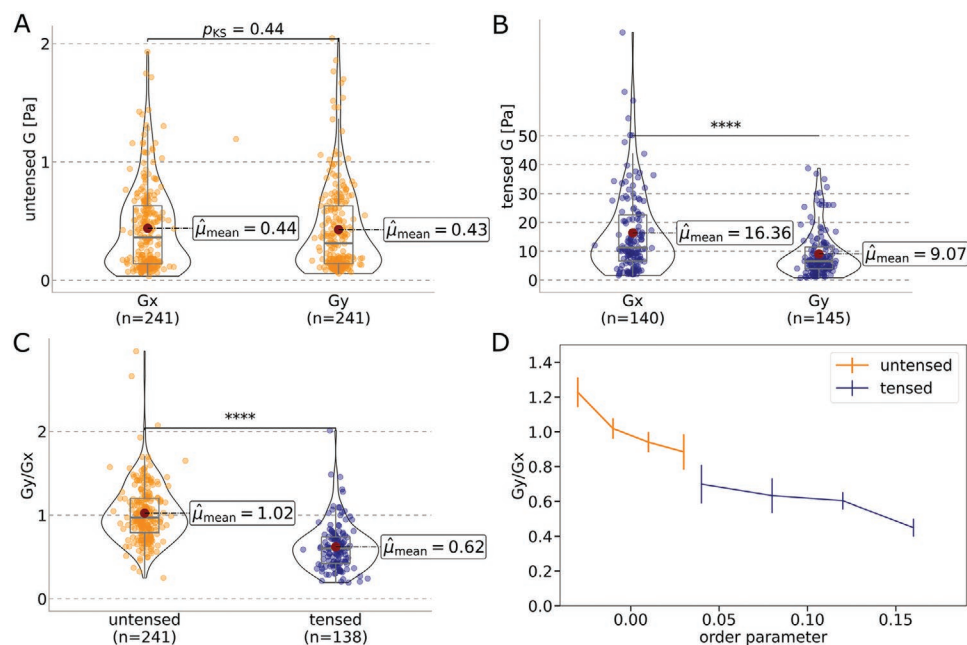


Figure 3. Local stiffness measurement of fibrin gels with 1-point active microrheology. A,B) Comparison of the shear modulus distributions in x - and y -directions, for untensed and tensed gels, respectively. C) Distributions of stiffness ratios G_y/G_x in untensed and tensed gels. Horizontal black lines represent Kolmogorov–Smirnov statistical tests, where **** corresponds to a p -value lower than 0.0001. D) Stiffness ratio as a function of the order parameter measured from confocal scans in the driven bead area. Trends display average \pm SEM of binned distributions.

is that the response to the perturbation is linear, that is, the oscillation amplitudes of each of the beads in the field of view are linearly proportional to the amplitude of the driven bead. We assume this is the case for both untensed and tensed gels. That is, the external tension triggers a nonlinear material response, and the small bead oscillations probe the modified environment after the response to tension, without an additional nonlinear effect. We validate this assumption by showing a similar response to different amplitudes of driven bead oscillations in Figure S7, Supporting Information. We also assume that for low frequencies the response is independent of the frequency (see Section 2.1). This assumption is justified in Figure S8, Supporting Information.

Videos S2 and S3, Supporting Information, display driven bead oscillations in the x and y directions, showing also the tracer beads' response. Figure 4 displays a typical example of quantification of tracer bead amplitudes, directions, and phases of oscillations in x and y for an isotropic, untensed gel. The measured oscillations qualitatively match Oseen's tensor structure, in which the amplitudes are larger along the axis of applied force. The phase differences obtained from Fourier analysis (Figure 4C,D) are distributed narrowly around zero, and are most-likely due to measurement limitations such as sampling frequency, rather than actual phase differences. The ratio of drive frequency to frame rate gives 12° phase difference per frame, so that errors around 12° are expected. These results demonstrate that in the absence of external tension, fibrin gels behave as predicted by Oseen's tensor, without any time-lag between the oscillations in different regions.

To get a reliable quantification of the response, normalized amplitudes of tracer beads from multiple videos are collected. Assuming a linear response of the medium, normalized amplitudes from different videos can be treated as independent measurements of the medium response, which can thus be

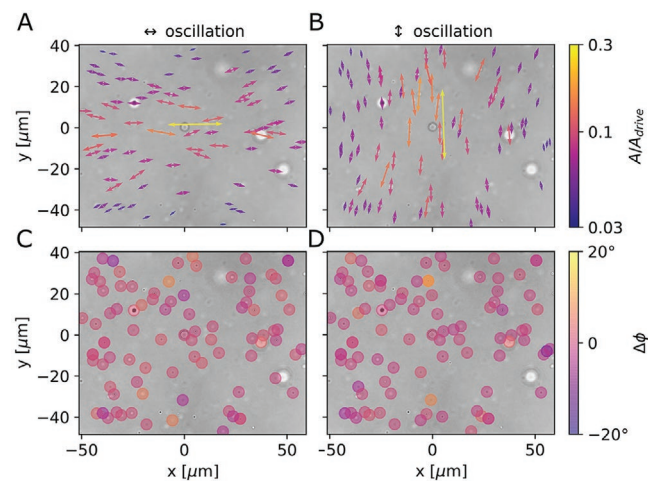


Figure 4. Example of an oscillation field obtained from analysis of a brightfield video in an untensed gel, with (A) displaying the response to an oscillation in the x -direction and (B) displaying the response to an oscillation in the y -direction. Arrow amplitudes are scaled up by a factor of 10, their direction represents the true oscillation direction, and their color represents their amplitude normalized by the driven bead amplitude. C,D) Plots showing the phase differences $\Delta\phi = \phi_{\text{tracer}} - \phi_{\text{driven}}$ corresponding to the oscillations in (A) and (B).

averaged. For clarity, we use the symbols \parallel and \perp to denote coordinates in parallel and perpendicular to the axis of tension. These are also used in the case of untensed gels, where \parallel and \perp simply denote two orthogonal directions.

To rule out possible artifacts in our setup or analysis, we first make sure that for isotropic gels we measure identical response in \parallel and \perp directions, and then check how this changes for tensed gels. Figure 5 shows collected amplitudes from 10–30 regions in each gel, from eight untensed (Figure 5A,B) and 13 tensed (Figure 5C,D) gels in total. First, we want to understand how the direction of the force with respect to the axis of tension affects force propagation. Thus, we separately quantify the response for oscillations along $x(\parallel)$ and $y(\perp)$. Figure 5E illustrates this part of the analysis, in which we average the response amplitudes \bar{U}_{\parallel} and \bar{U}_{\perp} over all angles (see Equation (3)), to obtain the “azimuth-averaged response” A_{\parallel} and A_{\perp} , in which \parallel/\perp denote the direction of oscillation with respect to the axis of tension. Figure 5F shows the decay of the A_{\parallel} and A_{\perp} , comparing tensed and untensed gels. For untensed gels, A_{\parallel} and A_{\perp} are approximately equal and are in a very good agreement with the prediction of Equation (3), shown as a solid black line. This indicates that the shear modulus in 1-particle and 2-particle measurements is indeed consistent, as was also shown in passive microrheology. This strengthens the conclusion that when beads are strongly adhered to the fibers, 1-point and 2-point microrheology gives similar results, unlike for non-adhering beads.^[46] We also verified the theoretical prediction that the off-diagonal elements of the displacement response tensor averages to zero when summing over all angles, for both tensed and untensed gels (see Figures S9 and S10, Supporting Information). For tensed gels, A_{\parallel} is reduced with respect to A_{\perp} by roughly 33% (Figure 5F), showing a substantial anisotropic response. In essence, this result means that when the gel is stretched along the x -axis, the transmission of parallel perturbations is largely reduced with respect to transmission of perpendicular perturbations. Also, for tensed gels the perturbation propagates with power dependence of ≈ -0.6 . This irregular behavior is consistent in all tensed gels, as shown in Figure S10, Supporting Information. This effect cannot be simply explained by anisotropy and we discuss possible reasons for this behavior in Section 2.5. To demonstrate that our results are robust, we compare the results for three tensed and three untensed gels (Figures S9 and S10, Supporting Information). We chose individual gels for which the amount of videos and collected data were sufficient for robust quantification of the response. In addition, we verified that our main findings are reproduced in gels with a concentration of 1 mg mL^{-1} , as shown in Figures S11 and S12, Supporting Information.

Figure 5G,H illustrates averaging over sectors (“pizza slices”) to obtain the “direction-averaged response” A_{ij} showing how a force in the i th direction propagates in the j th direction.

Figure 5I,J shows the directional response of untensed and tensed gels, respectively. Again, it can be seen that in untensed gels (Figure 5I) the response is in agreement with theory (Equation (4), denoted by dashed lines), and that the material response is isotropic—the two blue trends (response in the same direction as the oscillation, corresponding to blue sectors in Figure 5F,G) coincide, as well as the two orange trends

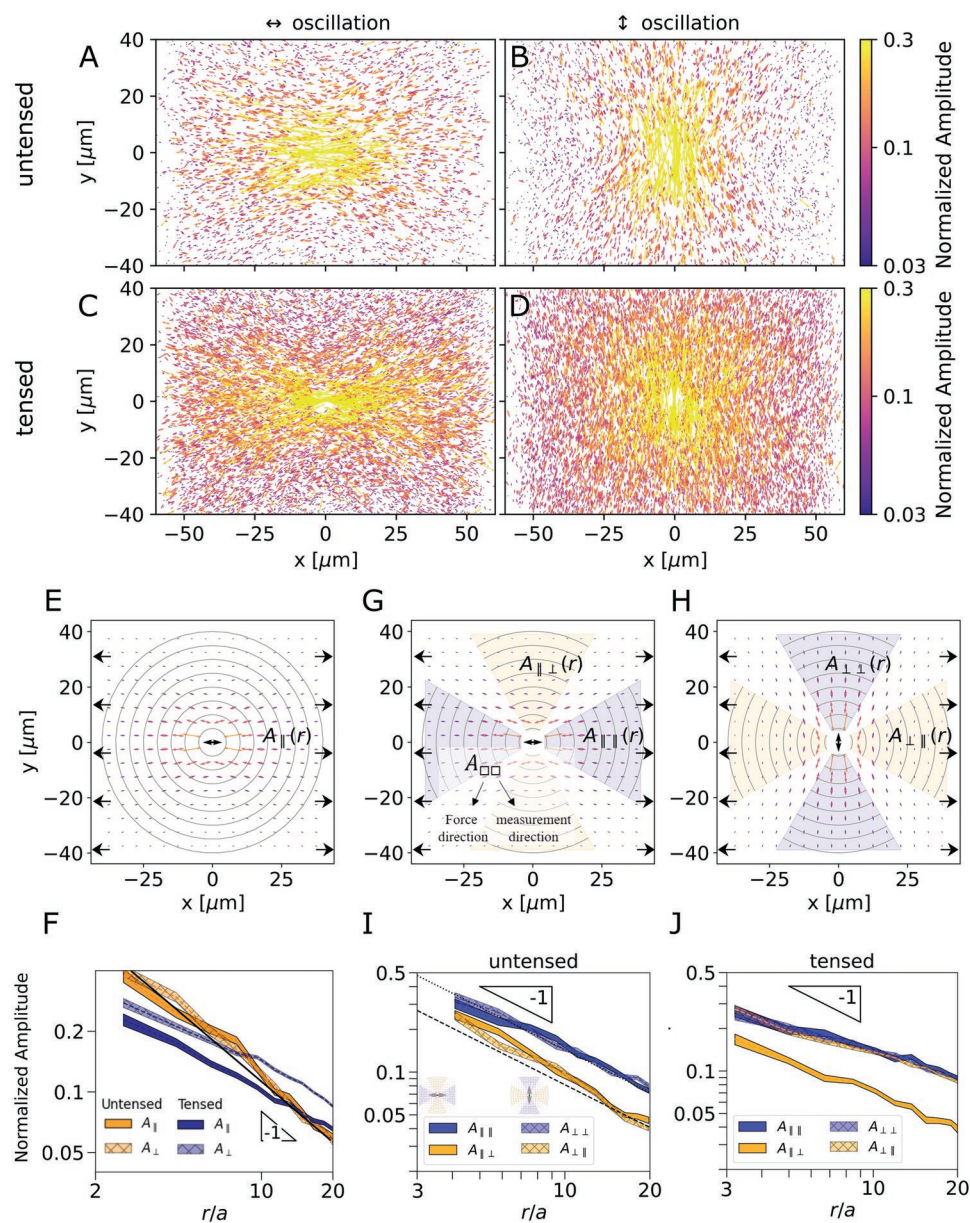


Figure 5. Oscillation fields collected from multiple gels and positions. A–D) Vector fields showing the response to oscillations in parallel (↔) and perpendicular (⊥) to the axis of tension, for untensed and tensed gels. E) The averaging scheme to obtain A_{\parallel} and A_{\perp} . The displacement field is shown schematically. The black arrows along the sides denote the axis of tension, and the double arrow in the center denotes the direction of drive oscillations. Concentric circles imply averaging over all angles. F) A_{\perp} and A_{\parallel} as a function of normalized distance from the driven bead. G, H) Directional analysis. Colored sectors (“pizza slices”) imply averaging over 60° sectors parallel and perpendicular to the axis of tension. Blue sectors are in the same direction as the oscillation, while orange sectors are perpendicular to it. Solid black line corresponds to the theoretical trend for isotropic materials (Equation (3)). I, J) The directional response, with the blue/orange trends corresponding to blue/orange sectors in (F) and (G). Dashed black lines in panel (I) correspond to theoretical trends for isotropic materials (Equation (4)). Trends display average \pm SEM.

(response perpendicular to the oscillation, corresponding to the orange sectors). From the ratios of the prefactors $A_{\parallel\parallel}/A_{\parallel\perp}$ and $A_{\perp\perp}/A_{\perp\parallel}$ for untensed gels, Poisson’s ratio can be estimated (see Equation (S8), Supporting Information). Fitting the trends yielded $\nu = 0.47 \pm 0.02$, in agreement with the incompressibility assumption and consistent with previous studies of fibrous gels’ microrheology.^[46,61]

In contrast, for tensed gels (Figure 5J) the directionality in the response changes in the following way: for a perturbation

parallel to the axis of tension, the response becomes more strongly oriented along that axis, such that the ratio $A_{\parallel\parallel}/A_{\perp\perp}$ becomes large compared to untensed gels (dark blue and dark orange trends are separated more than in the untensed gels). Moreover, for a perturbation perpendicular to the axis of tension, the response becomes nearly isotropic ($A_{\perp\perp} \approx A_{\perp\parallel}$; light blue and light orange trends overlap).

We can summarize these results as follows: for a tensed gel, the response to forces perpendicular to tension is amplified, but

the propagation *parallel to tension* is stronger, compared with isotropic gels.

To attempt and explain these observations, we combine previous theoretical studies of point-force response in anisotropic material. Head and Mizuno^[63] showed that tensed fibrous network have three independent elastic moduli. They also derived a generalization of Stokes' law for a force in perpendicular and parallel to the point force. We used their results, along with the solution of Pan and Chou to the Green's function of a transversely isotropic material.^[64] We choose a combination of elastic moduli that reproduces the results of our 1-point active microrheology (Figure 3B). We then compute the predicted displacements and perform the same analysis as for the experimental data. Results are shown in Figure S4, Supporting Information. The results qualitatively reproduce the increase in the ratio $A_{|||}/A_{||\perp}$ and the decrease in the ratio $A_{\perp\perp}/A_{\perp||}$ (Figure S4D, Supporting Information). However, the increase in the difference between A_{\perp} and $A_{||}$ is negligible for this theory (Figure S4C, Supporting Information), and the theory does not show any change in the power-law behavior. Thus, some, but not all of the experimentally observed effects are reproduced using the above computation.

2.5. Discussion

External tension is involved in a wide range of biological processes,^[25] and is known to alter the behavior of cells in various scenarios.^[26–29] External tension is often used in tissue engineering to train the tissue construct and achieve desired properties.^[65] Here, we studied how tension modifies the propagation of forces in a fibrous gel.

We have developed a framework for quantitative analysis of 1-point and 2-point microrheology of fibrous materials under tension. This is the first study, to our knowledge, that demonstrates the use of quantitative microrheology methods, and in particular 2-particle microrheology, for the study of fibrous gels under external tension. Therefore, it has the potential to push forward the understanding of mechanical communication between cells, which play a pivotal role in many fundamental biological processes including cell migration and proliferation.^[13,14,16,66,67] As most of our body tissues are constantly subject to external loads, it is of great importance to study the propagation of mechanical signals in tissues and tissue-mimicking gels under tension, as we do here.

Fibrin is a frequently studied fibrous hydrogel. Fibrin gels with similar composition to ours have been studied previously with rheology^[33,68] and microrheology.^[33] They showed that gels prepared with this concentration contain fibers with a diameter of ≈ 100 nm. They measured a storage modulus in agreement with ours. We combine three main approaches to quantify the changes in a fibrin gel induced by tension—confocal microscopy, 1-point microrheology, and 2-point microrheology. Confocal microscopy visualizes the structure of the gel in thin slices. It can be seen in the confocal images that the gels are very sparse, with large pores and fiber lengths with sizes comparable to the diameter of driven beads (≈ 3.43 μm). Image analysis showed that the mean pore size is ≈ 6 μm . Because Stokes' law assumes the medium is homogeneous, the large

mesh size raises questions as to the validity of 1-point microrheology in quantifying the shear modulus. Piechocka et al., who studied very similar fibrin gels,^[33] found large deviations between 1-point microrheology and bulk rheology. They measured similar values of shear moduli to ours using rheology, but smaller values using microrheology. Here, however, we found similar results in rheology, passive 1-point and 2-point microrheology, and somewhat smaller values in active 1-point microrheology. Our results show that 1-point and 2-point microrheology give the same shear modulus (Figure 1B, and also the agreement with theory in Figure 5H). As it seems, having the beads strongly adhered to the fibers enables microrheology to reliably probe the network's storage modulus. However, consistently with^[33] we find much smaller, effectively negligible loss modulus in microrheology at low frequencies (Figure 1B). This indicates that the large mesh size leads to negligible friction between the network and the solvent at small frequencies, making microrheology less sensitive to dissipation in the solvent compared to bulk rheology.

We also used active 1-point microrheology to quantify the stiffness of untensed gels. Values of G were somewhat lower in active microrheology compared with passive microrheology and bulk rheology. This small discrepancy most likely arises from underestimation of the trap stiffness, which was not measured in situ, but separately in water.

When tensed, the gel stiffens dramatically, by a factor of around 30. It was recently shown that tension causes much higher fiber alignment, molecular unfolding^[69] and stiffening^[30] compared to shear stress. Interestingly, this is in contrast to the fact that in AFM studies, individual fibrin fibers were shown to stiffen only by a factor of up to two under tensile strain.^[70] Therefore, it seems that network rearrangement due to tension, rather than the response of individual fibers, gives rise to dramatic stiffening. Moreover, densification due to compression along the z -axis may also contribute to stiffening. By image analysis, we estimated that the fiber volume fraction increases under tension by about a factor of 2 (see Figure S5, Supporting Information). The stiffness of untensed fibrous gels scales roughly quadratically with concentration, and this scaling argument implies stiffening by about a factor of 4. However, compression by a factor larger than 50% was shown to increase the stiffness by several orders of magnitude.^[57] It remains challenging to uncouple these effects. The fact that the ratio of parallel and transverse stiffness was about 1.8, suggests that the stiffness anisotropy can be attributed to individual fiber stiffening along the axis of tension, while the overall stiffening is due to network rearrangement in response to tension and compression.

Our results show that the local fiber alignment determines the material mechanical anisotropy, even if the overall structure of the gel is isotropic (see Figure 3D). This means that even in the absence of tension and nonlinear response of the fibers, local fiber orientation leads to mechanical anisotropy.

Next, we studied the effects of tension on force propagation. Our main microrheology setup, in which we use bright-field microscopy to track the tracer beads' oscillations in response to an active force applied by optical tweezers, has the advantage that a large amount of data is recorded with low noise, which allowed us to quantitatively match our results with

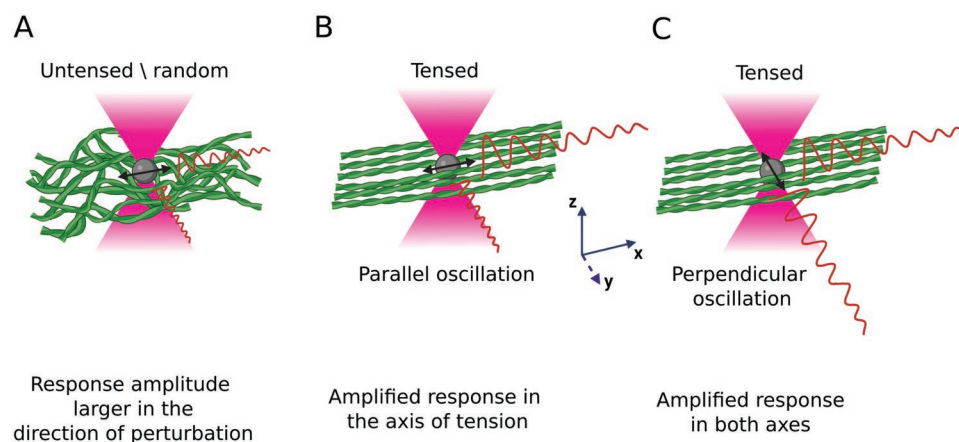


Figure 6. Illustration depicting the central results for 2-point active microrheology. A) A bead (gray) embedded in an untensed network with random fiber orientations is oscillated by optical tweezers (pink). The response amplitudes are larger along the axis of the oscillation, as shown by Oseen's tensor (Equation (2)). B) When the network is tensed, and the oscillation is along the axis of tension, the response amplitudes are even larger along the tensed axis. C) When the network is tensed, and the oscillation is perpendicular to the axis of tension, the amplitudes are enhanced along both axes.

theory, despite high material heterogeneity (see Figure 5). Another advantage is that large forces can be applied, thus pushing up the range of stiffness that we can probe. With this method, what effectively limits the stiffness range is that large forces require high laser power, which ultimately heats up the medium, causing drifts. A drawback of this method is that different frequencies need to be sampled one at a time, and high frequencies are not accessible due to the limited camera speed. Thus, active microrheology characterizes only the low-frequency plateau.

We used untensed fibrin gels as a control to test our setup and analysis. As expected, we found an isotropic response, with equal propagation of the signal regardless of the direction of the applied driven oscillation, with a characteristic $1/r$ decay trend. Our results are in qualitative agreement with a combination of Stokes' law and Oseen's tensor, assuming incompressible medium. This result is in agreement with our passive microrheology, which also shows that 1-point and 2-point shear moduli are equal, which is a central assumption in our analysis. From the comparison of force propagation parallel and perpendicular to the oscillation, we estimated Poisson's ratio, and found a value near $1/2$, consistent with previous studies.^[46,61]

There are several interesting effects that modify force propagation when the gel is put under tension, which were studied in this work for the first time. **Figure 6** illustrates the main findings. Panel (A) illustrates a bead oscillating in an untensed gel, in which the response is described by Oseen's tensor. Panel (B) depicts a bead oscillation in a tensed gel, with the oscillation parallel to the axis of tension, showing that the response along the axis of tension is enhanced. Panel (C) shows the situation in which the oscillation is perpendicular to the axis of tension. In this case, we found that the response is amplified in both axes.

We hypothesized that the renowned stiffening of fibrin gels should result in anisotropic transmission of mechanical signals. First, by averaging the response amplitudes over all angles, we found that the overall response to a force perpendicular to the axis of tension becomes stronger than the response to a force parallel to the axis of tension (Figure 5F). The elastic theory that we compared with did not show this effect. Yet another

interesting result is related to the force propagation directionality with respect to the direction of the driven oscillation. Oseen's tensor predicts that in untensed gels, displacements are larger in the direction of the applied force compared to displacements in the transverse direction ($A_{\parallel\parallel} = A_{\perp\perp} > A_{\perp\parallel} = A_{\parallel\perp}$, see Equation (4) and Figure 5I). In tensed gels, however, we find that for forces parallel to the axis of tension, the response becomes oriented in the direction of the force even more ($A_{\parallel\parallel}/A_{\perp\perp}$ increases) while it becomes less oriented when the force is perpendicular to the axis of tension ($A_{\perp\perp}/A_{\perp\parallel}$ decreases). We can say that in general, forces in tensed gels propagate further along the tensed axis. Here, the theoretical model gave a good qualitative agreement and also showed that $A_{\parallel\parallel}/A_{\perp\perp}$ should increase while $A_{\perp\perp}/A_{\perp\parallel}$ should decrease for a tensed gel (Figure S4, Supporting Information).

A surprising result was that displacements in tensed gels decayed with a power law exponent significantly smaller than -1 . This result could not be explained by the model described above. The usual cause for irregular power-law behavior is a non-linear response, but we also ruled this out by measuring a linear response to different amplitudes (see Section S7 and Figure S7, Supporting Information). We showed that this behavior is robust by demonstrating it on multiple gels (Figure S10, Supporting Information). One possible explanation is that tension in fibrous materials tends to create force-chains that can transmit force more efficiently.^[23,71,72] Recently, anomalous force propagation with a slow-decreasing power-law was observed in simulations of fibrous gels near their rigidity percolation point.^[73] Because external tension is known to lower the rigidity percolation point,^[32] this mechanism may explain our results if tension brings the gels close to their rigidity percolation transition. Further studies are required to pin-point the origins of this irregular behavior. Such changes of power-law can significantly increase the effective range of communication between cells.^[38,71]

The study of anisotropic materials, and especially their micromechanical properties, is very limited compared to the understanding of isotropic media. The simplest anisotropic elastic model that can describe a tensed gel, known as

transverse-isotropic material, has five elastic moduli,^[64,74] which can be reduced to three under physical assumptions on the mechanics of fibrous materials.^[63] By combining previous contributions and matching their predictions with our experimental results, we demonstrated that the available theory supports several aspects of our experimental results. It would be beneficial to extend the existing theory and explore ways to recover the moduli of anisotropic materials using microrheology. It also remains a challenge to determine these moduli macroscopically from bulk rheology or nano-indentation, and theoretical efforts are required so that anisotropic materials can be characterized and compared systematically. Here, we chose the elastic moduli in the model to fit the results of 1-point active microrheology.

Our central motivation was to better understand cell mechanical communication in fibrous materials under tension. Previous biological studies have shown that cancer cells aggregates, for example, can apply tension to fibrous gels and then take advantage of the induced fiber alignment for more efficient migration.^[16,75] In a pioneering study, Szulcowski et al.,^[54] showed that external tension leads to larger displacements along the axis of tension. They showed that cancer cells preferentially grow protrusions and migrate in the axis of tension. Importantly, they also measured displacement fields in the material in response to cell-applied forces, and found that displacements propagate further along the tensed axis. Their method is different than ours in several aspects, and their results, suggesting that cell communication is enhanced along the axis of tension, are in line with the findings of our directional analysis, showing that tension amplifies the propagation along the tensed axis. However, our study shows that the *direction of the force* is also important, and that forces perpendicular to the axis of tension are more strongly amplified. This finding is particularly important because cells are often polarized and apply highly directional forces.^[19] Another example of the importance of force direction was found by Nitsan et al.^[76] They showed that cardiac cells synchronized their beating with a mechanical device that locally oscillates the substrate, but only if the oscillations were perpendicular, and not parallel, to the cell long axis. These results as well as ours, highlight the importance of external tension and its relation to the direction of applied signal, to mechanical cell communication.

In summary, our study explores the consequences of tension to force propagation in fibrous gel. Our results suggest that tension dramatically modifies the mechanical properties and alters force propagation. These results can help elucidate processes that involve external and internal forces in fibrous networks, which are common in morphogenesis and tissue remodeling, such as in wound healing and tumor stroma. It may also help in designing protocols that involve external tension in tissue engineering.

3. Experimental Section

Fibrin Gel Preparation: Fibrin gel was prepared by mixing Fibrinogen (Evel Biopharmaceuticals) at a final concentration of 0.25 mg mL⁻¹ with Thrombin (Evel Biopharmaceuticals) at a final concentration of 1 U mL⁻¹. This sub-physiological concentration was chosen so that optical tweezers could substantially displace embedded driven particles,

and so the response was large enough to be measured across the entire 100 μm field of view, whilst avoiding high laser power that could heat and damage the sample. This concentration also allowed passive microrheology, which is limited to materials softer than ≈10 Pa.^[77] In Section S9, Supporting Information, results are also shown for gels with 1 mg mL⁻¹ fibrin.

Fibrinogen was fluorescently labeled with Alexa Fluor 546, succinimidyl ester (Invitrogen), as previously described.^[78] Prior to mixing of thrombin and fibrinogen, thrombin solution was supplemented with 0.005 wt% of 0.75 μm fluorescent beads (Fluoresbrite YG Carboxylate Microspheres, Polysciences) to serve as tracers, and 0.004 wt% of 3.43 μm beads (Spherotech) to serve as driven beads. The tracers are coated with carboxylate groups that adhere to proteins at physiological pH. For isotropic gels, the solution was mixed on top of a glass slide, and closed with another slide with 1 mm spacing. Gels that will be stretched were prepared on top of a parafilm strip, inside a circular mold cut into a silicone rubber strip of 1 mm thickness, as described previously.^[78,79] The gels polymerized over-night at 37 °C. After polymerization, the fibrin gel naturally adhered to the silicone strip, allowing gel straining through external stretch of the silicone.^[78,79]

Bulk Rheology: A Discovery HR-3 rheometer with a plate-plate geometry (20 mm diameter, 1mm gap) was used to characterize the macroscopic shear modulus of the gel at increasing degrees of strain. The gels were polymerized inside the rheometer for 3 h before measurements. A solvent trap was used in order to avoid gel dehydration during polymerization and measurement. The strain frequency was 0.5 Hz, matching the frequency in microrheology experiments. Frequency sweeps from 0.1 to 20 Hz were performed with a strain amplitude of 5%.

Passive Microrheology: Imaging the motion of the tracer particles within the gels was done using an Olympus IX71 epi-fluorescence microscope, at λ = 480 nm with a 60× oil objective. The motion of ≈250 particles were recorded in the field of view using a CMOS video camera (Grasshopper 3, Point Gray) at a frame rate of 30 Hz with an exposure time of 10 ms. Data from at least 10⁵ frames were used. Particle tracking was done by conventional video microscopy, using the protocol of Crocker and Grier.^[80] In 1-point microrheology, *G* was computed from the mean square displacement of individual tracer beads, and in 2-point microrheology it was computed from the correlated mean squared displacement of particle pairs. The algorithms for these computations were described previously.^[60,81] These methods measure the complex shear modulus $G = G' + iG''$ over a frequency range that was determined by the sampling frequency and video length, and in this case was from 1 to 20 Hz.

Loading of Gels into the Tensile Device: The tensile device used in this work was a simple metal frame with clamps on both sides and a holder for a glass slide in the middle (see Figure S1, Supporting Information). The device was made of an anodized aluminum plate which fits on the stage of the optical tweezers microscope (C-trap; LUMICKS). A hole with a diameter of 40 mm in the center of the plate allowed the microscope lens to approach the sample from below. Two screw-holes were drilled on each side of the plate. When the silicone strip with the gel was placed on the plate, its sides were clamped using two small aluminum clamps. Screws were used to tighten the clamps. To load the sample, a silicon strip including the gel was picked up from the box where it polymerized and the parafilm was removed. The silicone strip was then placed along the frame so that the gel was laying on the glass slide and the ends of the strip were under the clamps. The silicone strip was clamped on one side, and pulled manually from the other side so that the length of the hole enclosing the gel was increased by 50%. Based on a previous study by the authors,^[78] this was equivalent to about 40% strain in the bulk of the material. The other clamp was tightened, preventing the silicone from contracting back. The frame was then placed on the microscope stage and the gel was let to relax for 10 min before beginning the experiment. Within this setup, the axis of tension was always chosen as the x-axis of the microscope imaging. For isotropic gels, samples were prepared on a glass cover-slip, placed on the microscope stage and held with clamps.

Active Microrheology: A C-Trap confocal fluorescence optical tweezers setup (LUMICKS) made of an inverted microscope based on a

water-immersion objective (NA 1.2) together with a condenser top lens was used. The optical trap was generated by 10 W 1064-nm laser. The trap could be steered using a piezo mirror with a feedback mechanism to determine its accurate position. The samples were illuminated by a bright field 850-nm LED and imaged in transmission onto a metal-oxide semiconductor (CMOS) camera at a frame rate of 15 Hz. Each microrheology measurement consisted of focusing the trapping laser on a 3.5 micron bead, and driving it sinusoidally by oscillating the trapping laser once in the x -axis and once in the y -axis. To avoid boundary hydrodynamic effects, it was made sure that driven beads were at least 100 μm from the bottom glass and from gel edges. The trap stiffness κ was calibrated by fitting the power spectrum of beads trapped in water to a lorentzian.^[82] Calibration was done separately for each laser power used in the experiment. The trap stiffness was found to be independent on the height of the bead above the glass, as long as the bead was at least 100 μm above it. The drive frequency was 0.5 Hz to guarantee that measurements would be in the low-frequency plateau of the storage modulus (see Section 2.1), but avoiding unnecessarily long measurement times. The bead was oscillated for 10–20 s, giving 5–10 full oscillations. The drive amplitude was 1–2 microns (but was always equal in x and y), low enough to avoid nonlinear gel response (see Section S7, Supporting Information), but high enough to be detected across the field-of-view. The driven bead was tracked using a phase-modulated Hough transform with Matlab (The MathWorks, Inc.). The same method also yielded the bead radius a which was used in computations to prevent errors due to bead size dispersity. The material shear modulus G was estimated using Stokes' law for an isotropic, incompressible material, linking the displacement $\bar{u}^{(1)}$ of a bead of radius a subject to a force \bar{F} :

$$\bar{u}^{(1)} = \frac{1}{6\pi a G} \bar{F} \quad (1)$$

with the force given by $\bar{F} = \kappa(\bar{u}^{\text{trap}} - \bar{u}^{(1)})$, where \bar{u}^{trap} is the trapping laser displacement and κ is the trap stiffness.

Stokes' law assumes the material is homogeneous down to the scale of the bead. This assumption is unlikely to hold because gels had a mesh size larger than the bead size (see Figure S2, Supporting Information). Therefore, Stokes' law is expected to hold only on average. In addition, there might be a correction factor due to network compressibility (see Section S4, Supporting Information).

Simultaneously, tracer beads were tracked using the trackpy python package. The oscillation amplitudes of driven beads and tracer beads on both axes were found by taking the Fourier transform of their trajectory along the desired coordinates, and extracting its magnitude at the applied frequency. This effectively filtered out low-frequency drifts and high-frequency noise, leaving only the response to the applied perturbation. The accuracy of this method was tested by oscillating a 1.5 micron bead in water, as described in Figure S3, Supporting Information.

2-Point Active Microrheology Analysis: In order to suggest a framework for analyzing 2-particle microrheology in tensed gels, the suitable theory for isotropic fibrin gels was discussed first.^[60,84] When a force, \bar{F} is applied to a bead within a linearly elastic, isotropic, and incompressible medium, the displacement of a second bead at position $\bar{r} = (r_x, r_y)$ with respect to the driven bead is given by Oseen's tensor (shown here for $z = 0$):

$$\begin{bmatrix} u_x^{(2)}(r, \phi) \\ u_y^{(2)}(r, \phi) \end{bmatrix} = \frac{1}{8\pi r G} \begin{bmatrix} 1 + \cos^2(\phi) & \cos(\phi)\sin(\phi) \\ \cos(\phi)\sin(\phi) & 1 + \sin^2(\phi) \end{bmatrix} \begin{bmatrix} F_x \\ F_y \end{bmatrix} \quad (2)$$

with $r = |\bar{r}|$, $\phi = \arctan(r_y/r_x)$, and G is the shear modulus. To compare theoretical predictions to results, Equations (1) and (2) were combined, defining the "displacement response tensor" $\bar{U}(\bar{r})$ as $\bar{u}^{(2)}(\bar{r}) = \bar{U}(\bar{r})\bar{u}^{(1)}$. The response was then averaged over all angles (see Figure 5E) and get the "azimuth-averaged response" (derived in Section S4, Supporting Information):

$$\begin{bmatrix} A_x(r) \\ A_y(r) \end{bmatrix} \equiv \frac{1}{2\pi} \int_0^{2\pi} \begin{bmatrix} \bar{U}_{xx}(r, \phi) \\ \bar{U}_{yy}(r, \phi) \end{bmatrix} d\phi = \frac{9a}{8r} \begin{bmatrix} 1 \\ 1 \end{bmatrix} \quad (3)$$

the azimuth-averaged responses A_x and A_y are a measure of the overall response to a point force in the x and y directions, respectively. Their expression could be readily compared to experimental results because it does not include G . However, it relies on the assumption that G took the same value in Equations (1) and (2). In other words, it was assumed that local measurement of G (Equation (1)) would give the same result as a non-local measurement (Equation (2)), which is not always the case.^[46]

Equations (1) and (2) describe incompressible materials with Poisson's ratio $\nu = 1/2$. The corresponding expressions for compressible materials are given in the Section S4, Supporting Information.

Another important aspect of the response to oscillatory perturbation is the directionality of the displacement field. It was of interest to know whether there were directions in which the response was larger. This directionality was chosen to be described by averaging \bar{U} over sectors ("pizza slices") of $\pm 30^\circ$ to the principle axes x and y (illustrated in Figure 5G,H). It was shown in Section S4, Supporting Information, that for an isotropic, incompressible material, the average of the displacements in these $\pm 30^\circ$ sectors is:

$$\begin{bmatrix} A_{xx}(r) \\ A_{yy}(r) \end{bmatrix} \equiv \frac{3}{\pi} \int_{-\pi/6}^{\pi/6} \begin{bmatrix} \bar{U}_{xx}(r, \phi) \\ \bar{U}_{yy}(r, \phi) \end{bmatrix} d\phi = \frac{9a}{8r} \begin{bmatrix} 1 + \frac{\sqrt{3}}{2\pi} \\ 1 - \frac{\sqrt{3}}{2\pi} \end{bmatrix} \quad (4)$$

$$\begin{bmatrix} A_{xy}(r) \\ A_{yx}(r) \end{bmatrix} \equiv \frac{3}{\pi} \int_{-\pi/3}^{\pi/3} \begin{bmatrix} \bar{U}_{xx}(r, \phi) \\ \bar{U}_{yy}(r, \phi) \end{bmatrix} d\phi = \frac{9a}{8r} \begin{bmatrix} 1 - \frac{\sqrt{3}}{2\pi} \\ 1 + \frac{\sqrt{3}}{2\pi} \end{bmatrix}$$

A_{ij} was termed as the "direction-averaged response". The first index in A_{ij} indicated the direction of the point-force, and the second index indicated the direction of measurement (x or y axis). Thus, A_{ij} was used to measure how forces in different directions propagate along the two principal axes.

While it is customary to choose a coordinate system in which the two particles were aligned along the x -axis, here anisotropic gels which have fixed principal directions were studied. Throughout this paper, x was chosen as the axis along which the gel was tensed. The notations x/y and \parallel/\perp were used interchangeably to denote directions parallel and perpendicular to the axis of tension. The material response in Equation (2) has mirror symmetries $x \leftrightarrow -x$ and $y \leftrightarrow -y$, which caused the off-diagonal entries of the displacement response tensor, $\bar{U}_{xy}, \bar{U}_{yx}$, to average to zero in integrals such as in Equations (3) and (4). In a tensed gel, inversion symmetries will still hold as long as x, y were aligned with the principal directions of tension. However, isotropic gels also had rotational symmetry, which was broken in tensed gel. This could lead to differences between A_x and A_y , as well as between A_{xx} and A_{yy} and between A_{xy} and A_{yx} as shown in Section S4 and Figure S4, Supporting Information.

The material response was computed by collecting the positions and amplitudes of tracer beads from multiple positions and gels, normalizing them by the driven bead amplitude, and averaging over their values in concentric rings. The material surrounding the driven bead was divided into rings with 3 μm thickness, and the amplitude component was averaged in the direction of the applied oscillation, over each of these rings. A_x and A_y were obtained. Averaging the measured amplitudes over 60° sectors ("pizza slices") in the x and y directions was used to obtain the "direction-averaged responses" A_{xx}, A_{yy}, A_{xy} , and A_{yx} . This method was necessary in order to overcome the material heterogeneity, thus requiring to average over large sets of measurements to characterize the material response. For quantitative analysis, data were collected with 10–30 driven beads in each gel, and for 13 tensed and eight untensed gels. With that, A_{ij} could be reliably quantified in the range from 2 to 20 bead radii, limited by the field-of-view.

Confocal Fluorescence Microscopy: After recording each video of an oscillating driven bead, a fluorescent scan of the structure of the fiber network around the driven bead was also acquired, using the confocal laser scanner of the C-trap microscope (60 \times water objective). Scanning was done using a tip/tilt piezo mirror. Pixel size was 100 nm and pixel dwell-time was 0.1 μs . Photons were counted using fiber-coupled single-

photon counting modules. The multi-mode fibers served as pinholes providing background rejection. Two excitation lasers, of 488 nm (blue) and 561 nm (green), were used to excite the fluorescent labels of tracer beads and fibers, respectively. Time limitations precluded taking several image stacks for each bead, so only the focal plane of the driven bead was scanned.

To illustratively show how bead oscillations were propagated in the network, time-lapse recordings of a bead oscillation in a “move–pause–scan” manner (and not in real time) was taken—small consecutive displacements of the optical trap were performed, taking a confocal scan of the mesh after each small displacement.

To characterize the pore structure, Zeiss LSM 880 confocal microscope was used with an Airyscan detector, using 40× water immersion lens (Zeiss) with a 30-mW argon laser (wavelength 514 nm).

Quantification of Fiber Alignment and Densification: Confocal images taken with the C-trap confocal laser scan were used to estimate the alignment of fibers. A script in Matlab (Mathworks inc.) was used to extract fiber alignment. The green fluorescent label of the fibers was used for this analysis. Local intensity gradients g_x , g_y were calculated for each pixel by convolution of the image with 21X21 Sobel operator, and the fiber orientation was calculated as $\theta = \tan^{-1}(g_x/g_y)$. The nematic order parameter (NOP) was calculated as

$$\text{NOP} = \langle \cos 2\theta \rangle \quad (5)$$

The nematic order parameter varies between -1 and 1 , with 1 corresponding to full alignment in the x -direction, 0 corresponding to random orientation, and -1 corresponding to full alignment in the y -direction.

Confocal images were used also to determine whether tensed gels were denser compared to untensed gels. This was done in Matlab by binarizing the images with Otsu's method,^[85] and computing the number of white pixels. It was expected that this simple measure was proportional to the volume fraction occupied by fibers.

Number of Samples and Statistics: Bulk rheology was performed over five gel samples. Passive microrheology was averaged over ten different regions of the same sample. Active microrheology was done on eight untensed and 13 tensed gels, and from each gel 10–20 driven beads were oscillated, to a total of 270 driven beads for untensed gels and 218 beads for tensed gels. For every bead both x and y oscillations were recorded. Each video had in the order of 100 tracer particles. 1-point active microrheology was done using the same video as 2-point active microrheology, using 198 driven beads for untensed and 145 driven beads for tensed gels. Confocal microscopy scans of the regions around driven beads were recorded for six untensed and nine tensed, resulting in 198 regions for untensed gels and 151 for tensed gels.

To determine whether two measured distributions (for example, shear modulus distributions) are distinguishable, Kolmogorov–Smirnov test was used. This test made no previous assumptions about the underlying distributions. In all figures, **** indicates p -value (p_K) less than 10^{-4} .

Code Availability: The main code files used for this project are available via: <https://github.com/shahargoren/2p-microrheology-of-tensed-gels.git>. Sample data to experiment with this code are available upon request.

Supporting Information

Supporting Information is available from the Wiley Online Library or from the author.

Acknowledgements

A.L. and R.S. jointly supervised this work. The authors are grateful to Haim Diamant, Yael Roichman, Naomi Oppenheimer, and Yair Shokef

for illuminating discussions. The authors thank Sudheer Kumar Cheppali for help with graphics editing. R.S. acknowledges support by the ISRAEL SCIENCE FOUNDATION (grant no. 1289/20). A.L. acknowledges support by the ISRAEL SCIENCE FOUNDATION (grant no. 1474/16) and the Israeli Centers for Research Excellence (grant no. 1902/12).

Conflict of Interest

The authors declare no conflict of interest.

Data Availability Statement

The data that support the findings of this study are available from the corresponding author upon reasonable request.

Keywords

fibrin, force propagation, mechanical cell communication, microrheology, tension

Received: April 25, 2022
Revised: October 31, 2022
Published online: November 26, 2022

- [1] C. Frantz, K. M. Stewart, V. M. Weaver, *J. Cell Sci.* **2010**, *123*, 4195.
- [2] C. Storm, J. J. Pastore, F. C. MacKintosh, T. C. Lubensky, P. A. Janmey, *Nature* **2005**, *435*, 191.
- [3] A. J. Licup, S. Münster, A. Sharma, M. Sheinman, L. M. Jawerth, B. Fabry, D. A. Weitz, F. C. MacKintosh, *Proc. Natl. Acad. Sci. USA* **2015**, *112*, 9573.
- [4] C. S. Roy, *J. Physiol.* **1881**, *3*, 125.
- [5] E. Bell, B. Ivarsson, C. Merrill, *Proc. Natl. Acad. Sci. USA* **1979**, *76*, 1274.
- [6] K. A. Jansen, R. G. Bacabac, I. K. Piechocka, G. Koenderink, *Biophys. J.* **2013**, *105*, 2240.
- [7] D. E. Discher, P. A. Janmey, Y.-I. Wang, *Science* **2005**, *310*, 1139.
- [8] Y. Tony, P. C. Georges, L. A. Flanagan, M. Beatrice, O. Miguelina, F. Makoto, Z. Nastaran, M. Wenyu, W. Valerie, P. A. Janmey, *Cell Motility* **2004**, *60*, 24.
- [9] A. J. Engler, S. Sen, H. L. Sweeney, D. E. Discher, *Cell* **2006**, *126*, 677.
- [10] C. M. Lo, H. B. Wang, M. Dembo, Y. L. Wang, *Biophys. J.* **2000**, *79*, 144.
- [11] V. Panzetta, S. Fusco, P. A. Netti, *Proc. Natl. Acad. Sci. USA* **2019**, *116*, 22004.
- [12] Y. Wang, G. Wang, X. Luo, J. Qiu, C. Tang, *Burns* **2012**, *38*, 414.
- [13] T. Korff, H. G. Augustin, *J. Cell Sci.* **1999**, *112*, 3249.
- [14] P. Pakshir, M. Alizadehgiashi, B. Wong, N. M. Coelho, X. Chen, Z. Gong, V. B. Shenoy, C. McCulloch, B. Hinz, *Nat. Commun.* **2019**, *10*, 1850.
- [15] S. C. Schwager, P. V. Tafalele, C. A. Reinhart-King, *Cell. Mol. Bioeng.* **2018**, *12*, 1.
- [16] Q. Shi, R. P. Ghosh, H. Engelke, C. H. Rycroft, L. Cassereau, J. A. Sethian, V. M. Weaver, J. T. Liphardt, *Proc. Natl. Acad. Sci. USA* **2014**, *111*, 658.
- [17] R. S. Sopher, H. Tokash, S. Natan, M. Sharabi, O. Shelah, O. Tchaicheeyan, A. Lesman, *Biophys. J.* **2018**, *115*, 1357.
- [18] X. Ma, M. E. Schickel, M. D. Stevenson, A. L. Sarang-Sieminski, K. J. Gooch, S. N. Ghadiali, R. T. Hart, *Biophys. J.* **2013**, *104*, 1410.

- [19] M. S. Hall, F. Alisafaei, E. Ban, X. Feng, C.-Y. Hui, V. B. Shenoy, M. Wu, *Proc. Natl. Acad. Sci. USA* **2016**, *113*, 14043.
- [20] X. Xu, S. A. Safran, *Phys. Rev. E* **2015**, *92*, 32728.
- [21] Y. Shokef, S. A. Safran, *Phys. Rev. Lett.* **2012**, *108*, 178103.
- [22] H. Wang, A. Abhilash, C. S. Chen, R. G. Wells, V. B. Shenoy, *Biophys. J.* **2014**, *107*, 2592.
- [23] S. Goren, Y. Koren, X. Xu, A. Lesman, *Biophys. J.* **2020**, *118*, 1152.
- [24] B. Burkel, J. Notbohm, *Soft Matter* **2017**, *13*, 5749.
- [25] W. Zhang, G. Huang, F. Xu, *Front. Bioeng. Biotechnol.* **2020**, *8*, 589590.
- [26] S. Toume, A. Gefen, *Int. Wound J.* **2017**, *14*, 698.
- [27] K. Shikano, K. Chiba, S. Miyata, *Adv. Biomed. Eng.* **2015**, *4*, 170.
- [28] B. Maleiner, J. Tomasch, P. Heher, O. Spadiut, D. Rünzler, C. Fuchs, *Front. Physiol.* **2018**, *9*, 1130.
- [29] N. F. Jufri, A. Mohamedali, A. Avolio, M. S. Baker, *Vascular Cell* **2015**, *7*, 8.
- [30] A. S. Van Oosten, M. Vahabi, A. J. Licup, A. Sharma, P. A. Galie, F. C. MacKintosh, P. A. Janmey, *Sci. Rep.* **2016**, *6*, 19270.
- [31] P. A. Janmey, M. E. McCormick, S. Rammensee, J. L. Leight, P. C. Georges, F. C. MacKintosh, *Nat. Mater.* **2006**, *6*, 48.
- [32] A. Sharma, A. J. Licup, K. A. Jansen, R. Rens, M. Sheinman, G. Koenderink, F. C. MacKintosh, *Nat. Phys.* **2016**, *12*, 584.
- [33] I. K. Piechocka, R. G. Bacabac, M. Potters, F. C. MacKintosh, G. Koenderink, *Biophys. J.* **2010**, *98*, 2281.
- [34] K. A. Jansen, A. J. Licup, A. Sharma, R. Rens, F. C. MacKintosh, G. Koenderink, *Biophys. J.* **2018**, *114*, 2665.
- [35] D. A. Vader, A. Kabla, D. A. Weitz, L. Mahadevan, *PLoS One* **2009**, *4*, e5902.
- [36] J. Feng, H. Levine, X. Mao, L. M. Sander, *Phys. Rev. E: Stat., Nonlinear, Soft Matter Phys.* **2015**, *91*, 042710.
- [37] F. C. MacKintosh, J. Käs, P. A. Janmey, *Phys. Rev. Lett.* **1995**, *75*, 4425.
- [38] J. Notbohm, A. Lesman, P. Rosakis, D. A. Tirrell, G. Ravichandran, *J. R. Soc., Interface* **2015**, *12*, 20150320.
- [39] P. Ronceray, C. P. Broedersz, M. Lenz, *Proc. Natl. Acad. Sci. USA* **2016**, *113*, 2827.
- [40] P. Rosakis, J. Notbohm, G. Ravichandran, *J. Mech. Phys. Solids* **2014**, *85*, 16.
- [41] J. Feng, H. Levine, X. Mao, L. M. Sander, *Soft Matter* **2016**, *12*, 1419.
- [42] C. P. Broedersz, F. C. MacKintosh, *Rev. Mod. Phys.* **2014**, *86*, 995.
- [43] F. C. MacKintosh, C. Schmid, *Curr. Opin. Colloid Interface Sci.* **1999**, *4*, 300.
- [44] R. M. Robertson-Anderson, *ACS Macro Lett.* **2018**, *7*, 968.
- [45] A. Sonn-Segev, A. Bernheim-Groswasser, Y. Roichman, *Soft Matter* **2014**, *10*, 8324.
- [46] M. L. Gardel, M. T. Valentine, J. C. Crocker, A. R. Bausch, D. A. Weitz, *Phys. Rev. Lett.* **2003**, *91*, 8.
- [47] M. Shayegan, N. Rezaei, N. H. Lam, T. Altindal, A. Wiczorek, N. R. Forde, *Proc. SPIE* **2013**, *8810*, 88101P.
- [48] M. Levin, P. Sorkin, D. Pine, R. Granek, A. Bernheim-Groswasser, Y. Roichman, *Soft Matter* **2020**, *16*, 7869.
- [49] M. Shayegan, N. R. Forde, *PLoS one* **2013**, *8*, e70590.
- [50] H. Lee, J. M. Ferrer, F. Nakamura, M. J. Lang, R. D. Kamm, *Acta Biomater.* **2010**, *6*, 1207.
- [51] C. A. R. Jones, M. Cibula, J. Feng, E. A. Krnacik, D. H. McIntyre, H. Levine, B. Sun, *Proc. Natl. Acad. Sci. USA* **2015**, *112*, E5117.
- [52] Y. L. Han, P. Ronceray, G. Xu, A. Malandrino, R. D. Kamm, M. Lenz, C. P. Broedersz, M. Guo, *Proc. Natl. Acad. Sci. USA* **2017**, *115*, 4075.
- [53] M. A. Kotlarchyk, S. G. Shreim, M. B. Alvarez-Elizondo, L. C. Estrada, R. Singh, L. Valdevit, E. Kniazeva, E. Gratton, A. J. Putnam, E. L. Botvinick, *PLoS one* **2011**, *6*, 5.
- [54] J. M. Szulcowski, D. R. Inman, M. Proestaki, J. Notbohm, B. M. Burkel, S. M. Ponik, *Acta Biomater.* **2021**, *129*, 96.
- [55] A. Parekh, D. Velegol, *Ann. Biomed. Eng.* **2007**, *35*, 1231.
- [56] T. Neckernuss, L. K. Mertens, I. Martin, T. Paust, M. Beil, O. Marti, *J. Phys. D: Appl. Phys.* **2016**, *49*, 045401.
- [57] R. I. Litvinov, J. W. Weisel, *Matrix Biol.* **2017**, *60*, 110.
- [58] W. Liu, L. M. Jawerth, E. A. Sparks, M. R. Falvo, R. R. Hantgan, R. Superfine, S. T. Lord, M. Guthold, *Science* **2006**, *313*, 634.
- [59] J. M. Zuidema, C. J. Rivet, R. J. Gilbert, F. A. Morrison, *J. Biomed. Mater. Res., Part B* **2014**, *102*, 1063.
- [60] J. C. Crocker, M. T. Valentine, E. R. Weeks, T. Gisler, P. D. Kaplan, A. G. Yodh, D. A. Weitz, *Phys. Rev. Lett.* **2000**, *85*, 888.
- [61] G. H. Koenderink, M. Atakhorrami, F. C. MacKintosh, C. F. Schmidt, *Phys. Rev. Lett.* **2006**, *96*, 138307.
- [62] J.-P. Collet, H. Shuman, R. E. Ledger, S. Lee, J. W. Weisel, *Proc. Natl. Acad. Sci. USA* **2005**, *102*, 9133.
- [63] D. A. Head, D. Mizuno, *Phys. Rev. E: Stat., Nonlinear, Soft Matter Phys.* **2013**, *88*, 2.
- [64] M. Kachanov, B. Shafiro, I. Tsukrov, in *Handbook of Elasticity Solutions*, Springer, Dordrecht **2003**, pp. 1–25.
- [65] B. D. Riehl, J. H. Park, I. K. Kwon, J. Y. Lim, *Tissue Eng., Part B* **2012**, *18*, 288.
- [66] R. Sunyer, V. Conte, J. Escribano, A. Elosegui-Artola, A. Labernadie, L. Valon, D. Navajas, J. M. Garcia-Aznar, J. J. Muñoz, P. Roca-Cusachs, X. Trepat, *Science* **2016**, *353*, 6304.
- [67] A. M. Valencia, P. H. Wu, O. N. Yogurtcu, P. Rao, J. DiGiacomo, I. Godet, L. He, M. H. Lee, D. Gilkes, S. X. Sun, D. Wirtz, *Oncotarget* **2015**, *6*, 43438.
- [68] E. A. Ryan, L. F. Mockros, J. W. Weisel, L. Lorand, *Biophys. J.* **1999**, *77*, 2813.
- [69] Y. Wang, S. Kumar, A. Nisar, M. Bonn, M. K. Rausch, S. H. Parekh, *Acta Biomater.* **2021**, *121*, 383.
- [70] W. Liu, C. R. Carlisle, E. A. Sparks, M. Guthold, *J. Thromb. Haemostasis* **2010**, *8*, 1030.
- [71] P. Ronceray, *Ph.D. Thesis*, Université Paris-Saclay, **2016**.
- [72] A. Mann, R. S. Sopher, S. Goren, O. Shelah, O. Tchaicheeyan, A. Lesman, *J. R. Soc., Interface* **2019**, *16*, 20190348.
- [73] E. Lerner, E. Bouchbinder, *arXiv:2209.04237*, **2022**.
- [74] S. Lekhnitskii, *Theory of Elasticity of an Anisotropic Body*, Mir Publishers, Moscow **1981**.
- [75] H. Ahmadzadeh, M. R. Webster, R. Behera, A. M. Jimenez Valencia, D. Wirtz, A. T. Weeraratna, V. B. Shenoy, *Proc. Natl. Acad. Sci. USA* **2017**, *114*, E1617.
- [76] I. Nitsan, S. Drori, Y. E. Lewis, S. Cohen, S. Tzilil, *Nat. Phys.* **2016**, *12*, 472.
- [77] T. A. Waigh, *Rep. Prog. Phys.* **2005**, *68*, 685.
- [78] A. Roitblat Riba, S. Natan, A. Kolel, H. Rushkin, O. Tchaicheeyan, A. Lesman, *Ann. Biomed. Eng.* **2020**, *48*, 868.
- [79] A. Kolel, A. Roitblat Riba, S. Natan, O. Tchaicheeyan, E. Saias, A. Lesman, *J. Visualized Exp.* **2020**, *166*, e61671.
- [80] J. Crocker, D. Grier, *J. Colloid Interface Sci.* **1995**, *179*, 298.
- [81] M. Levin, A. Sonn-Segev, Y. Roichman, *J. Chem. Phys.* **2019**, *150*, 64908.
- [82] K. Berg-Sørensen, H. Flyvbjerg, *Rev. Sci. Instrum.* **2004**, *75*, 594.
- [83] D. B. Allan, T. Caswell, N. C. Keim, C. M. van der Wel, R. W. Verweij, *soft-matter/trackpy: Trackpy v0.5.0* **2021**, <https://zenodo.org/record/4682814>.
- [84] A. J. Levine, T. C. Lubensky, *Phys. Rev. Lett.* **2000**, *85*, 1775.
- [85] N. Otsu, *IEEE Trans. Syst., Man, Cybern.* **1979**, *9*, 62.